Carrier Transit Time Approximation for Prediction of PETT Oscillation in Power Diodes

Michael Heeb[1)], Frank Pfirsch[2)], Thomas Hunger[3)], Oliver Schilling[3)], Peter Zacharias[1)]

[1]Uni Kassel / FB 16, IEE-EVS, Wilhelmshöher Allee 71, D-34121 Kassel, Germany
[2] Infineon Technologies AG, Am Campeon 1-12, D-85579 Neubiberg, Germany
[3] Infineon Technologies AG, Max-Planck-Straße 5, D-59581 Warstein Germany
Tel.: +49-561-804-6477 Fax:+49-561-804-6521 Email: Michael.Heeb@uni-kassel.de

Abstract

The occurrence of Plasma Extraction Transit Time oscillations under certain conditions in high power semiconductors is investigated experimentally and theoretically. The experimentally obtained data allow for detailed studies of influencing parameters and are compared with theoretical models from the literature predicting the oscillation frequency. Refinements on the models are carried out for better matching the experimental findings. The accuracy of the oscillation prediction is improved.

1. Introduction

During the turn-off phase of a high power semiconductor high frequency oscillations can appear under special conditions. They spread out into the close vicinity of the device and possibly cause EMC disturbances. One type of high frequency oscillation is known as the Plasma Extraction Transit Time (PETT) effect occurring within the tail phase [1]. There are several measures to avoid these electromagnetic disturbances [2].

Models for predicting the oscillation frequencies by studying the behavior of charge carriers in the semiconductor are reported [3]. In the present work a refined model for the prediction of the oscillation frequency is presented. The theoretical approach is supported by extensive experimental findings.

2. Reference Measurements on Diode Substrate

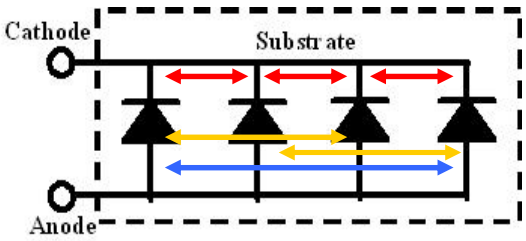

Fig. 1 Schematic of substrate with four paralleled 1700V power diodes

For reference purposes measurements on a substrate with four paralleled 1700V power diodes is carried out (fig. 1).

Fig. 2 shows a typical PETT oscillation occuring during the tail phase of the diode current (red line) measured by two antennas (green and blue line) at a diode voltage of U_{CC} = 350V. Three independent oscillations with different frequencies are visible. Each of them can be related to one of three possible resonance circuits: the small-sized resonance circuits (fig. 1, red arrows) located between adjacent diodes, the middle-sized circuits (fig. 1, yellow arrows) located between next nearest diodes and a large-sized one (fig. 1, blue arrow) located between the outer diodes.

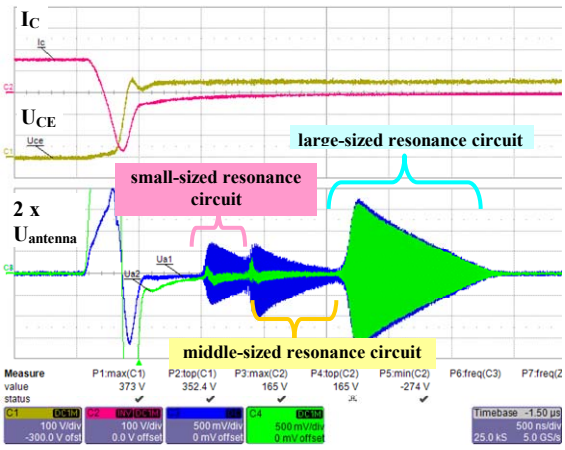

Fig. 2 Example of a typical PETT oscillation taken at U_{CC}= 350V, I_C= 150A & T_j= 300K

In fig. 3 the measurement points of the oscillation frequencies taken at different DC link stray inductances L_K are congruent. Accordingly, changes in inductance far from substrate do not influence the resonance behavior. Therefore, it is likely that only the parasitic inductances on the substrate together with the diode capacitances govern the oscillation frequencies.

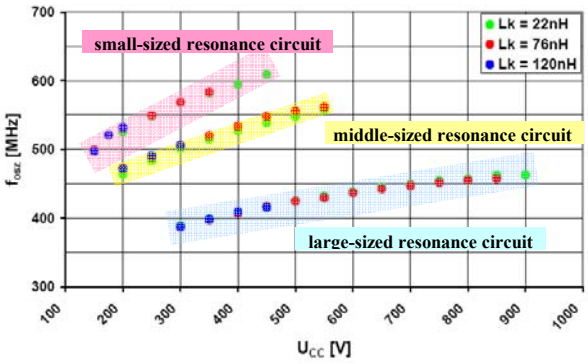

Fig. 3 Measured oscillation frequencies at different DC link stray inductance L_k taken at I_C = 150A and T_j = 25°C

One clearly recognizes from fig. 3 that the resonance frequency increases with increasing DC link voltage. Due to the frequencies measured the skin depth in the conductors (bond wires, DCB metallization) is smaller than the diameters of the conducting structures. Hence, constant parasitic inductances are assumed. The voltage dependence of the frequencies is then only governed by the voltage dependent diode capacitance as

$$C \sim 1/\sqrt{U_{CC}}$$
$$f_{osc} \sim 1/\sqrt{LC} \sim U_{CC}^{1/4} \qquad (1)$$

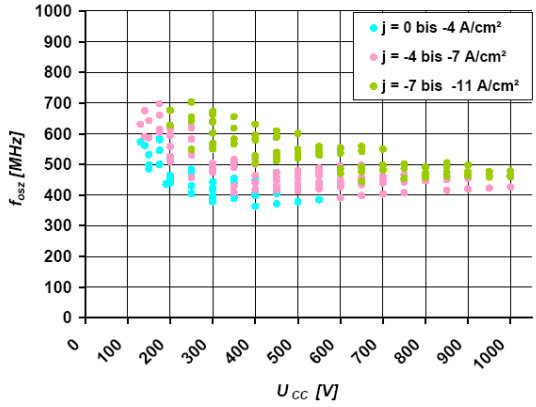

Fig. 4 Results of the substrate measurements: PETT-frequency f_{osz} as a function of the DC link voltage V_{CC} at different tail current heights j.

The oscillation frequencies are extracted by a FFT analysis from the experimental waveforms. The bond wire layout is changed several times for realizing a multitude of different resonance circuitries on substrate level by varying the inductances. As a result, a widespread of measurement points for the PETT oscillation frequency is found. The tail current density j measured just before the onset of the oscillations is analyzed (fig. 4). This provides an additional parameter used in the models below.

3. Prediction of the oscillation frequency range

In the tail current phase the space charge region is already established. At the cathode side of the device a plasma consisting of charge carriers still exists. The characteristic transit time for holes through the space charge region is denoted as t_T. According to the Ramo-Shockley-Theorem an oscillatory behavior is expected within a frequency range given by [4]:

$$\frac{1}{2t_T} \le f_{osc} \le \frac{1}{t_T} \qquad (2)$$

There are different models to calculate the carrier transit time t_T that are discussed below.

3.1. Constant hole velocity

Assuming a width w_{sc} for the space charge region and a constant velocity v_{sat} (saturation velocity) of the holes, the following equation is a common approximation for t_T [4,5]:

$$t_T = \frac{w_{SC}}{v_{sat}} \quad \text{with} \quad v_{sat} = 1 \cdot 10^7 \frac{cm}{s} \qquad (3)$$

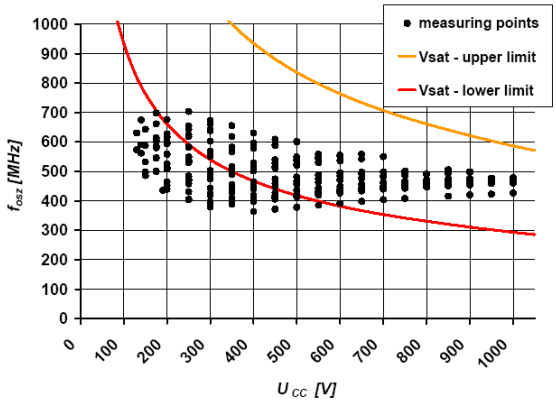

Fig. 5 Measured oscillation frequencies compared with the range limits given by the approximation of a constant hole velocity

The dependence of the resonance frequency on the applied DC voltage is governed by the rise of w_{sc} with increasing external voltage. In fig. 5 the allowed frequency range according to eqns. (2) and (3) are plotted and compared with the experimental findings. Only a part of the measured data is within the calculated limits. The theoretical prediction overestimates the frequency range.

The hole drift velocity does not reach the saturation value. This is considered as one of the reason for the discrepancy found. Furthermore, the injection and acceleration phase is not included in this simple approximation.

3.2. Consideration of space dependent hole velocity

The general formula for the field dependence of the drift velocity of holes is given by

$$v_{d,p} = \frac{v_{sat}}{1+\frac{E_m}{E(x)}} \qquad (4)$$

with an electric field constant E_m [1]. For getting the carrier transit time, the reciprocal of the hole velocity must be integrated in the limits of the space charge region width.

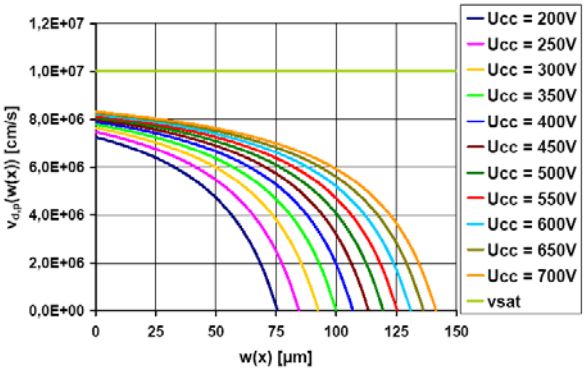

Fig. 6 Hole drift velocity distribution for different voltages U_{cc} applied externally. The saturation velocity v_{sat}=10^7 cm/s (green) is shown for comparison.

Under the condition of a triangular shaped electric field E(x) (Schottky approximation), the solution of the integral is given by the following equation:

$$t_T = \int_0^{w_{SC}} \frac{1}{v(x)_d}\,dx = \int_0^{w_{SC}} \left(\frac{1+\frac{E_m}{E(x)}}{v_{sat}}\right) dx \qquad (5)$$

$$= \frac{w_{SC}}{v_{sat}} + \frac{E_m \cdot w_{SC}}{E_{\max} \cdot v_{sat}} \cdot \ln \frac{w_{SC} - w_{SC}}{-w_{SC}}$$

with E_{max} being the electric field strength maximum at x=0 (center of the pn junction).

The resulting equation is divergent in the logarithmic term and hence cannot be used for a frequency determination. The reason for the divergence is plausible: for $x \rightarrow w_{sc}$ one gets $v_{d,p} \rightarrow 0$, which then leads to a divergent contribution of $1/v_{d,p}$ in the integral. The spatial dependence of the hole drift velocity in the space charge region is plotted in fig 6 for clarity.

3.3. Influence of finite tail current on charge density

So far, the finite tail current was not considered. It is now incorporated as a constant hole current density j_p. The Poisson equation has to be modified by introducing the positive charge of the holes given by $j_p/v_{d,p}$:

$$\frac{j_p}{v_{d,p}} = q \cdot p = \frac{j_p}{v_{sat}}\left(1+\frac{v_{sat}}{\mu_p E}\right) \qquad (6)$$

and

$$\rho = q\left(p + N_D\right). \qquad (7)$$

Substituting eqns. (6) and (7) into the one-dimensional Poisson equation results in

$$\frac{dE}{dx} = \frac{\rho}{\varepsilon_r \varepsilon_0} = \frac{j_p}{\varepsilon_r \varepsilon_0 \mu_p E} + \frac{qN_D + \frac{j_p}{v_{sat}}}{\varepsilon_r \varepsilon_0} \qquad (8)$$

$$= \frac{a}{E} + b$$

with the concentration of donators N_D, the specific and the relative permittivity $\varepsilon_0\varepsilon_r$, the elementary charge q and the mobility of free holes μ_p [6]. Transposing eqn. (8) with respect to dx

$$dx = \frac{E}{a} \cdot \frac{1}{1+\frac{bE}{a}} \cdot dE \qquad (9)$$

and integrated along the electric field E considering the initial conditions. As a result, the width of the space charge region is:

$$w_{SC} = \frac{E_{\max}}{b} - \frac{a}{b^2} \ln\left(1+\frac{bE_{\max}}{a}\right). \qquad (10)$$

The integration of eq. (9) also leads to the equation for the voltage as a function of maximum electric field E_{max}

$$U = \frac{1}{b}\left(\frac{E_{\max}^2}{2} - \frac{aE_{\max}}{b} + \frac{a^2}{b^2} \ln\left(1+\frac{bE_{\max}}{a}\right)\right) \qquad (11)$$

and the equation of the carrier transit time

$$t_T = \frac{1}{b v_{sat}} \left(E_{\max} + \left(\frac{v_{sat}}{\mu_p} - \frac{a}{b} \right) \ln\left(1 + \frac{b E_{\max}}{a} \right) \right). \quad (12)$$

The carrier transit time in eq. (12) is evaluated assuming E = 0 at the beginning of the space charge region next to the plasma boundary. The electric field at the beginning of the space charge region, and even in the plasma region, is larger than 0 in reality. Therefore, the equation overestimates the carrier transit time. For adjusting the carrier transit time it is assumed that the holes start at a point where the diffusion current of holes $j_{p,diff}$ at the end of the remaining plasma equals the field current j_p of the space charge region

$$j_{p,diff} = j_p . \quad (13)$$

The diffusion current of holes is related to the field current by

$$j_{p,diff} = -qD_p \frac{dp}{dx} \quad (14)$$

with elementary charge q, hole density p and diffusion constant of the holes D_p. Inserting eq. (6)

$$q \cdot p = \frac{j_p}{v_{d,p}} \quad \text{and}$$

$$\frac{D_p}{v_{d,p}} = \frac{V_T}{E} \quad (15)$$

with the thermal voltage V_T, in eq. (14) delivers

$$j_{p,diff} = \frac{j_p V_T}{E^2} \frac{dE}{dx} . \quad (16)$$

Substituting the one-dimensional Poisson equation and eq. (6) into eq. (16) results in

$$j_{p,diff} = j_p \frac{q V_T}{\varepsilon \varepsilon_o E^2} (p + N_D) . \quad (17)$$

Eqns. (12) and (17) lead to the electric field E_0 at the beginning of the space charge region and, E_0 inserted in eq. (11), to a correction term t_0 for the carrier transit time

$$t_{corr} = t_T - t_0 . \quad (18)$$

Including the hole current j_p new limits for the frequency range are deduced which are lower than the simple approximation taking into account only v_{sat} (fig. 7). The evaluated limits underestimate the measured frequency range.

The discrepancy between the measured data lying outside the estimated range and the upper limit, however, is much lower than in the simple approximation from above. The agreement with the measurements is improved considerably.

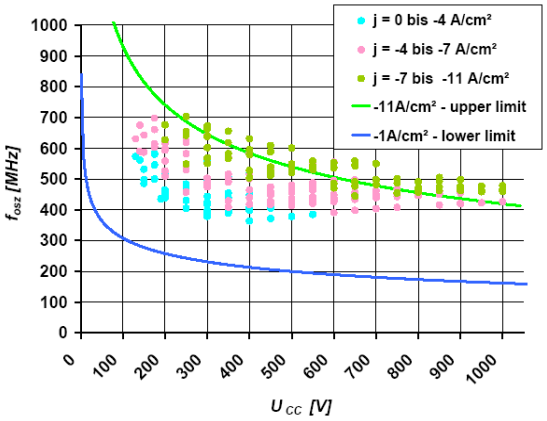

Fig. 7 Measured oscillation frequencies compared with the range limits from the approximation including the finite tail current j_p

4. Simulation of the oscillation frequencies

For verifying the measurement results and confirming the three resonance circuits assumed so far the substrate layout is rebuilt in Ansoft Q3D Extractor [7]. With the help of this software tool it is possible to extract the parasitic resistances, capacitances and inductances of the substrate layout. Because Q3D Extractor cannot simulate the semiconductors themselves, the device simulator Medici [8] was utilized to calculate the diode capacitance as a function of the DC link voltage U_{CC}. Fig. 8 shows the simulated diode capacitance which differs slightly from analytical results. Thus, the analytical calculations are considered as approximations only. The simulation considers the hole current density j_p and the oscillation frequency f_{osc} in addition to U_{CC}.

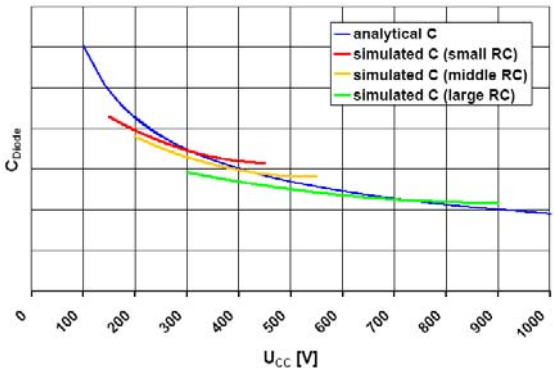

Fig. 8 Comparison between the analytically calculated and simulated diode capacitances.

In a subsequently performed small signal analysis using the Spice circuit simulator Simetrix [9] the equivalent circuits of the three resonance cir-

cuits are modeled independently. Finally, they are analyzed by a frequency sweep.

Fig. 9 shows the circuit under study. The substrate parasitics are according to the results from Q3D Extractor (dashed box) and given as a T-model. The diodes are represented by their capacitance values, C_1 and C_2. Changing U_{CC} needs the adjustment of the diode capacitances according to the results shown in fig. 8.

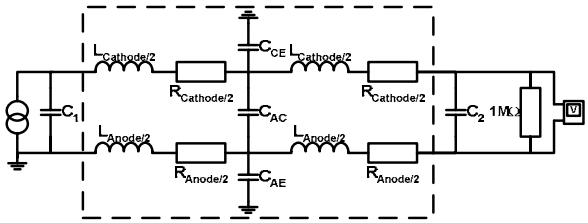

Fig. 9 RLC circuit of substrate model (dashed box) and the two diodes C_1 and C_2 as used for AC sweep analysis in Spice.

The frequency of the current source on the left side is swept while a voltage probe on the other side is plotting the resulting voltage amplification. At amplifications far beyond 1 the resonance frequency of the simulated circuit is detected.

Fig. 10 shows the results of the simulation in comparison to the experimental data. The deviations between simulation and measurement do not exceed more than 5%. The match between the experimental and the simulated data proofs the consistence of assuming three independent resonance circuits on the substrate.

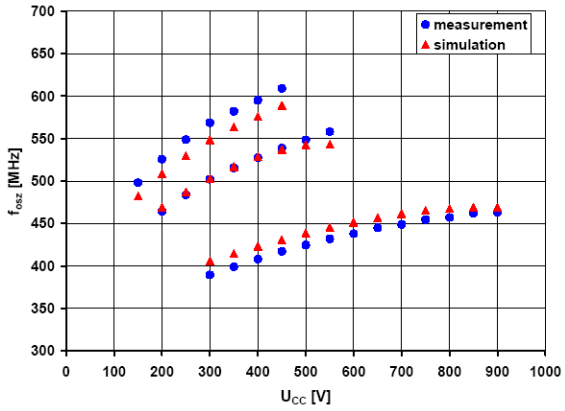

Fig. 10 Comparison between the measured data and the simulation results.

5. Conclusion

The paper presents extensive experimental and theoretical results on PETT oscillations on power diodes. Different models for predicting the oscillation frequencies are discussed that fit the experimental findings with different levels of accuracy. It is shown that the calculation of the frequency range incorporating the influence of current density is closer to the measurement data than the approximation based on a constant hole velocity.

Three different resonance circuits are found experimentally. Using simulations of the parasitics the circuits on substrate level are identified.

The higher confidence reached using the proposed models seems to improve the feasibility of a prediction of possible occurrence of PETT oscillations in an earlier stage of development where no prototypes are available. Thus, the quality and reliability of the power semiconductors is improved.

Next steps of the work are the extension of this investigation to other layouts to ensure the quality of the methodology.

6. Literature

[1] B. Gutsmann, P. Mourick, D. Silber: Plasma Extraction Transit Time Oscillations in Bipolar Power Devices, Solid State Electronics Vol. 46 Issue 1, January 2002, 133-138

[2] B. Gutsmann: Charakterisierung und Einfluß parasitärer elektromagnetischer Effekte in leistungselektronischen Bauelementen, PhD Thesis, University Bremen, 2006, 133-145

[3] S. Kitamura, T. Yamaguchi, H. Kondo, Y. Yamaguchi, M. Honsberg: The optimum design technology for turn-off oscillation avoidance, Proc. PCIM Europe 2007

[4] H. Eisele, G. Haddad: Active microwave diodes, in S.M. Sze, Modern semiconductor device physics, Wiley & Sons 1998, 343-402

[5] J. Lutz: Halbleiter-Leistungsbauelemente, Springer-Verlag, 2006, 366-374

[6] J.-F. Luy: Microwave semiconductor devices, Expert Verlag, 2006, 41

[7] www.ansoft.com

[8] www.synopsys.com

[9] www.simetrix.co.uk